Neuron, Vol. 32, 1165–1179, December 20, 2001, Copyright ©2001 by Cell Press

Response Correlation Maps of Neurons in the Mammalian Olfactory Bulb

Minmin Luo[1] and Lawrence C. Katz
Howard Hughes Medical Institute and
Department of Neurobiology
Duke University Medical Center
Durham, North Carolina 27710

Summary

To define the relationship between glomerular activation patterns and neuronal olfactory responses in the main olfactory bulb, intracellular recordings were combined with optical imaging of intrinsic signals. Response correlation maps (RCMs) were constructed by correlating the fluctuations in membrane potential and firing rate during odorant presentations with patterns of glomerular activation. The RCMs indicated that mitral/tufted cells were excited by activation of a focal region surrounding their principal glomerulus and generally inhibited by activation of more distant regions. However, the structure of the RCMs and the relative contribution of excitatory and inhibitory glomerular input evolved and even changed sign during and after odorant application. These data suggest a dynamic center-surround organization of mitral/tufted cell receptive fields.

Introduction

Sensory systems assign neuronal populations to process different portions of sensory information. The area upon which sensory stimulation elicits responses in a neuron is defined as the neuron's receptive field (Mountcastle, 1957). The neuronal receptive fields in somatosensory, auditory, and visual systems are well defined. In the visual system, for example, the receptive field can refer to a spatial location on the retinal surface or a range of wavelengths (DeMonasterio, 1979; Kuffler, 1953).

Historically, the receptive field of olfactory neurons in the main olfactory bulb has been defined in two ways. Firstly, it has been defined spatially as an area of olfactory epithelium that, upon odorant application (Kauer and Moulton, 1974) or electrical stimulation (Jiang and Holley, 1992), elicits activity change in postsynaptic neurons in the olfactory bulb. Neurons in the olfactory bulb respond to stimulation over widespread epithelial areas, suggesting broad receptive fields. The olfactory receptive field has also been defined as a set of odorants that elicits responses in bulbar neurons (Mori and Shepherd, 1994; Wilson, 2001). Particular features of molecular structures, such as carbon chain length or functional groups, modulate neuronal responses (Doving, 1966; Imamura et al., 1992; Katoh et al., 1993; Wilson, 2000). These properties probably reflect in large part the binding properties of the olfactory receptor themselves, and have provided critical insights into the neuronal coding of molecular shapes.

Results from recent anatomical and imaging studies suggest a different approach to define olfactory receptive fields. Individual epithelial neurons express only one olfactory receptor and neurons expressing the same receptors converge onto a few glomeruli in the olfactory bulb (Malnic et al., 1999; Mombaerts et al., 1996; Vassar et al., 1994). Odorants activate discrete domains, corresponding to individual glomeruli in the glomerular layer of the vertebrate olfactory bulb (reviewed in Xu et al., 2000), suggesting that odorant identities are initially mapped as spatial activation patterns in the glomerular layer of the bulb. In principle, the entire set of glomeruli, like the complete retinal surface, can be defined and quantified in terms of its responses to sensory stimuli. Activation of a discrete glomerular area by odorant application, as revealed by optical imaging, is conceptually similar to activation of a small retinal area by light projection. Thus, the relationship between the spatial locations of activated glomeruli and the cellular response of olfactory bulb neurons can be used to construct response correlation maps (RCMs), which are analogous to the concept of a receptive field in odor space.

Sophisticated receptive field mapping techniques have demonstrated that receptive fields in many sensory systems are not purely spatial or static, but have spatiotemporal structures and intrinsic dynamics (Dawis et al., 1984; Jenison et al., 2001; Jones and Palmer, 1987). Odorants elicit complex temporal patterns in the projection neurons of the vertebrate olfactory bulb (Friedrich and Laurent, 2001; Hamilton and Kauer, 1989; Wellis et al., 1989) and similarly complex spatiotemporal patterns within a large population of neurons in the salamander olfactory bulb (Cinelli et al., 1995; Kauer, 1988). Similar to the use of reverse correlation analysis for mapping receptive fields of neurons in the visual pathway (Jones and Palmer, 1987), the stimulus-evoked responses of mitral/tufted cells at different time points can be correlated with the spatial location of activated glomeruli to examine the spatiotemporal structures of the RCMs.

We used the relationship between glomerular spatial activation patterns and neuronal olfactory responses to construct RCMs and then examined the time-varying structure within these maps. By combining optical imaging of intrinsic signals and intracellular recordings, we found that the RCMs of mitral/tufted cells exhibited a center-surround organization, while those of granule cells were much more broad. Detailed analysis of time-varying changes of mitral/tufted cell RCMs revealed a gradual progression toward the center-surround organization but marked changes both during the initial phase of odorant pulses and immediately following the termination of odorant presentations.

Results

Optical imaging of intrinsic signals was used to image glomerular activation patterns on the dorsal surface of

[1]Correspondence: luo@neuro.duke.edu

both olfactory bulbs of adult mice (n = 22). Because of the requirement of long intervals between odorant presentations and the time constraints imposed by intracellular recording, 4–6 odorants were tested during the initial phase of optical imaging to generate maps of intrinsic signals. The functional domains of aldehydes (3–6 carbon chain length) were located within the central or anterior area of the dorsal bulb; heptanal and octanal activated anterior and slightly lateral areas; acetates (3–5 carbon) activated lateral or lateral and anterior parts of the bulb (Belluscio and Katz, 2001). Targeted intracellular recordings and neurobiotin injections were carried out following intrinsic signal imaging; cell types were subsequently identified by their morphology and soma location in histological sections. A total of 34 mitral cells, 7 tufted cells, and 10 granule cells were recorded from the dorsal surface of the bulb and 7 mitral cells were recorded from the ventral surface. Most neurons were held with small hyperpolarizing currents (<0.2 nA).

We first present the results of response patterns of mitral/tufted cells and the architecture of their RCMs, as determined by correlating the intrinsic signal patterns with intracellularly recorded odorant responses. We then present the results of additional analyses in which we assess the dynamics of these RCMs by correlating the spatial patterns of intrinsic signals with the electrophysiological responses of mitral/tufted cells over time. Lastly, we examine the architecture of granule cell RCMs.

Response Patterns of Mitral/Tufted Cells

Odorants evoked response patterns in mitral/tufted cells that could be roughly classified as either excitatory or inhibitory (Margrie et al., 2001). However, the temporal patterns were more subtle and could be further divided into subcategories (Hamilton and Kauer, 1989; Meredith, 1986; Wellis et al., 1989). Different odorants evoked distinct response profiles consisting of mixtures of excitatory and inhibitory subthreshold potentials and action potentials both during and after odorant pulses. An example of one neuron is shown in Figure 1. Propanal and butanal, which activated glomeruli immediately superficial to and anterolateral to the recording site, depolarized the cell and evoked vigorous spiking (Figures 1B_1, 1B_2, 1C_1, and 1C_2). Excitation was preceded by a brief, small hyperpolarization and ceased within 2 s following the end of odorant pulses. Heptanal, a longer hydrocarbon chain aldehyde, activated glomeruli 500–800 μm anterior to the recording site and strongly inhibited the cell. The inhibitory response consisted of membrane potential hyperpolarization and reduced spiking activity during odorant application. Brief depolarization and firing of action potentials synchronized with the breathing cycle were frequently observed riding on top of the inhibitory responses (Figure 1B_3). Following the end of heptanal pulses, the neuron rapidly depolarized and fired vigorously for several seconds (Figures 1B_3 and 1C_3). This cell was not obviously affected by propyl acetate and was inhibited by butyl acetate, which activated the lateral part of the bulb (Figures 1B_4–1B_5 and 1C_4–1C_5).

The soma of this cell was located within the dorsal mitral cell layer directly beneath the electrode penetration site. Its basal dendrites extended widely within the external plexiform layer (Figure 1D_1). The apical dendrite terminated in a glomerulus located ~280 μm anterior and ~180 μm lateral to the soma (Figure 1D_2), within the region anterior and lateral to the electrode penetration site that was activated by both butanal and propanal, but not by heptanal, propyl acetate or butyl acetate. The rostral tilting of mitral cell apical dendrites has been previously observed in rats (Buonviso et al., 1991).

More than two cells were recorded from the same olfactory bulbs at widely separated locations (n = 8 olfactory bulbs). Response profiles changed dramatically when the recording locations were shifted so that cells from different locations exhibited different response patterns to the same odorants. However, response profiles remained consistent with the spatial relationship between recording sites and activated glomeruli. In addition to the cell shown in Figure 1, two more cells were recorded from the same olfactory bulb. One was located posterior and another anterior and lateral to the cell shown in Figure 1 (Figure 2A). Heptanal evoked strongly excitatory responses in the cell located in the anterior part of the bulb (Figure 2C), while it evoked clearly inhibitory responses in both cells located posteriorly (Figures 1B_3 and 2B). Similarly, butanal evoked a vigorous excitatory response in the cell located in the middle (Figure 1B_2), but it had little effect on the cells located in the anterior and posterior parts of the bulb (Figures 2B and 2C).

In addition to mitral cells, a total of seven tufted cells were recorded, three of which were less than 100 μm below the glomerular layer. The response profiles of tufted cells resembled those of mitral cells. The response profiles are illustrated by a superficial tufted cell recorded from the anterior and lateral part of the bulb (Figure 3). Heptanal (1%) activated areas surrounding the recording site and strongly excited the cell (Figures 3B_2 and 3C_2). The other three odorants tested, butanal (1%), butyric acid (1%), and peanut butter, elicited an initial brief excitation and subsequently inhibited the cell to varying degrees (Figures 3B_1, 3B_3, 3B_4, 3C_1, 3C_3, and 3C_4). All of these odorants elicited off-responses following the end of odorant pulses.

Unlike mitral cells, many tufted cells (n = 4/7), and especially the superficial tufted cells (n= 3 /3), exhibited prolonged activation that lasted up to 2 min following 2 s of odorant stimulation (Figure 3D). These responses consisted of depolarization and vigorous spiking during each inhalation. All-or-none spikes of smaller amplitudes (<20 mV) and short duration (half amplitude duration = ~2 ms) were often observed during activation (Figure 3D inset). These small spikes persisted during an applied hyperpolarization that suppressed large action potentials, suggesting that they were fast pre-potentials originating from dendrites (Mori et al., 1982).

Response Correlation Maps of Mitral/Tufted Cells

The strong relationship between the spatial patterns of glomerular activation and the response profiles of mitral/tufted cells suggested that the overall field of responsive glomeruli could be defined by neuronal olfactory responses and the spatial location of activated glomeruli. To construct response correlation maps (RCMs) of mitral/tufted cells, we correlated the intracellular electrical responses to the spatial pattern of optically recorded

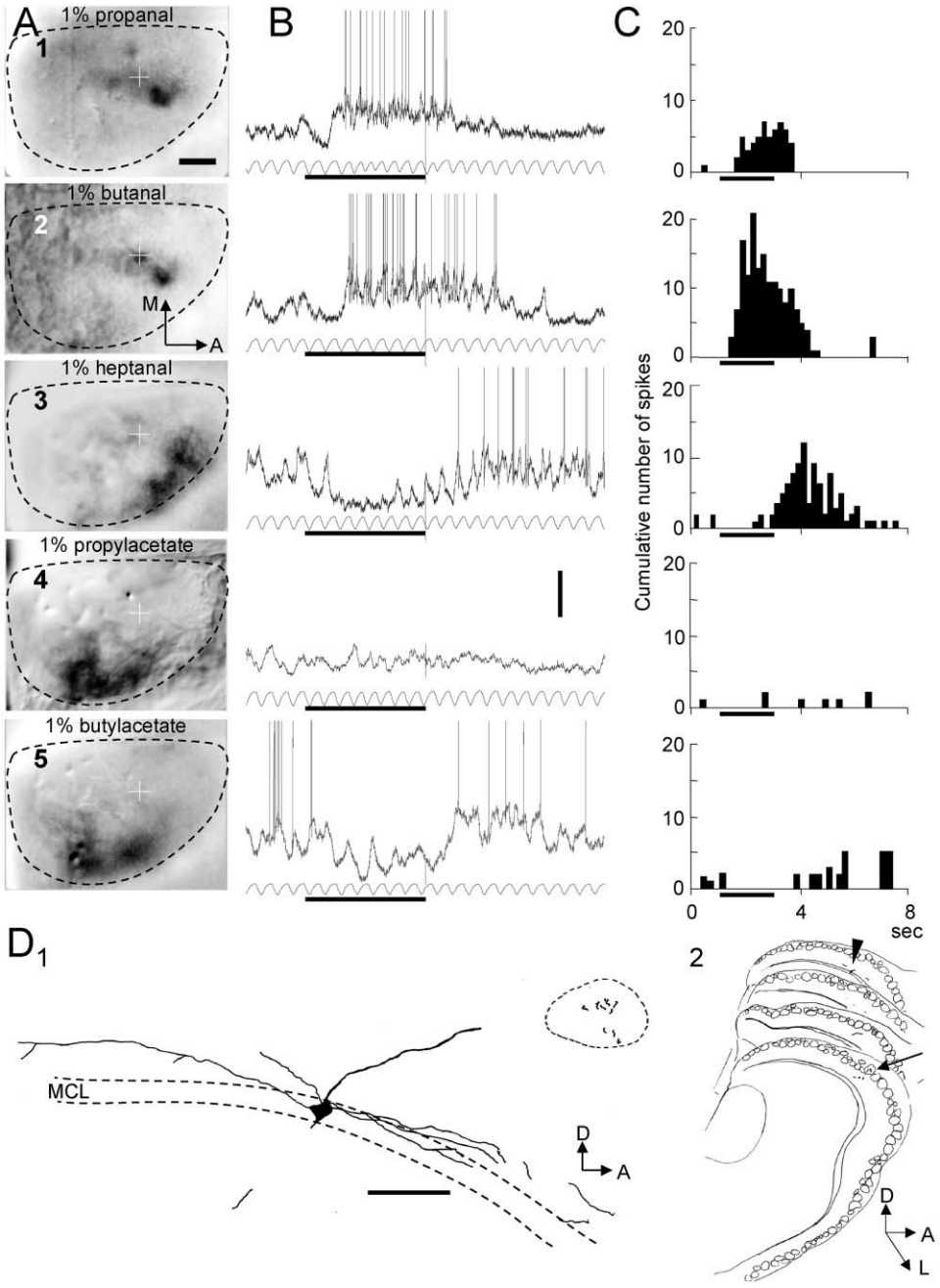

Figure 1. Glomerular Activation Patterns and Intracellularly Recorded Response Profiles of Mitral Cells

(A) Intrinsic signal maps of responses to five odorants that activated glomeruli on the dorsal surface of the olfactory bulb. Dashed lines indicate the border of the bulb. Crosshairs indicate the electrode penetration site, which was centered on a butanal responsive glomerulus. Bar = 500 μm. (B) Traces of an intracellularly recorded mitral cell in response to the same odorants used for imaging. This cell was strongly excited by propanal and butanal, strongly inhibited by heptanal and butyl acetate, and did not respond to propyl acetate. Breathing rhythm of the animal was monitored simultaneously and is shown below the traces of membrane potential. Horizontal bars under the traces of breathing rhythm indicate the timing of odorant pulses (2 s). The brief negative events at the end of odorant pulses are artifacts of solenoid closure. Action potentials were trimmed in this and following figures unless otherwise specified. Vertical bar = 10 mV. (C) Peri-stimulus time histogram of neuronal spiking activity in seven trials in response to the same odorants shown in (B). Note the initial inhibition followed by excitation in the propanal and butanal responses, and the pronounced off-responses to heptanal. (D_1) Camera lucida drawing of the recorded cell, the soma of which was situated in the mitral cell layer (MCL). Dashed closed line indicates the border of the glomerulus containing the tuft of this cell's apical dendrite. Bar = 100 μm. (D_2) Four serial parasagittal sections (60 μm thick) containing the cell's soma and apical dendrites. Its soma lay directly beneath the electrode penetration site and its apical dendrite tilted ~280 μm rostrally from its soma and 180 μm laterally from the section containing the soma. Arrowhead points to the location of soma and arrow points to the location of the tuft of the apical dendrite.

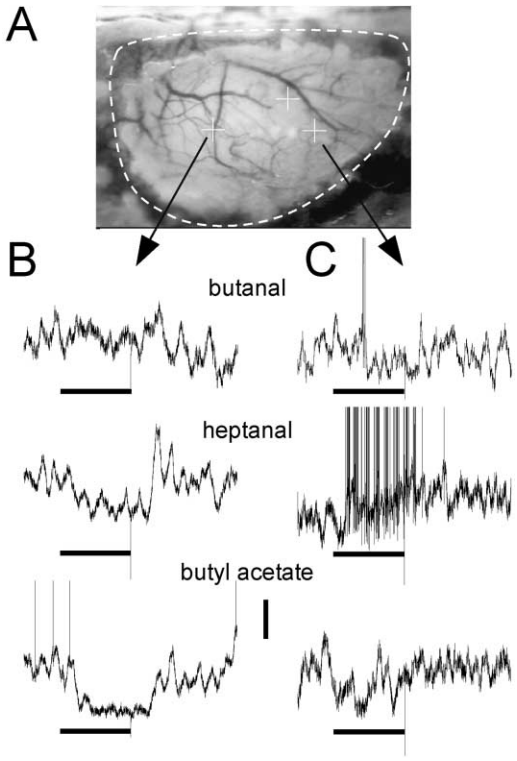

Figure 2. The Response Profiles of Mitral Cells Vary According to Their Spatial Relationship to Activated Glomeruli

(A) Blood vessel image of the same olfactory bulb shown in Figure 1 and the locations of electrode penetration sites. Dashed white line indicates the border of exposed olfactory bulb. Arrows indicates the traces of mitral cells recorded from dorsal mitral cell layer at locations indicated by crosshairs. The crosshairs without an arrow indicates the electrode penetration site for the mitral cell shown in Figure 1. (B) Sample traces of a cell in the posterior part of bulb in response to butanal, heptanal, and butyl acetate. Note that butanal evoked little response in this cell although it strongly excited the cell shown in (A). (C) Sample traces of a cell in the anterior and lateral part of bulb in response to the same odorants as in (B). Heptanal, which activated the anterior part of the bulb (Figure 1), strongly excited this cell but inhibited the cell shown in (B) and Figure 1. Horizontal bars in (B) and (C) = 2 s of odorant pulses. Vertical bars in (B) and (C) = 5 mV.

domains activated by odorants using a method conceptually similar to, but mathematically distinct from, reverse correlation (see Experimental Procedures and Figure 4). The RCMs described here are distinct from the receptive region in the epithelium or the molecular receptive range. Rather, they are analogous to a receptive field defined in the visual system by randomly stimulating small retinal regions whose spatial locations are correlated with the activity change of recorded neurons (Jones and Palmer, 1987).

In these RCMs of mitral/tufted cells, the effect of the activated glomeruli was correlated with the mean neuronal responses (either membrane potential change or firing frequency change) elicited by the odorant. Figure 4A illustrates the RCM for the cell shown in Figure 1, where the glomerular areas activated by propanal and butanal were excitatory (red to white) and areas activated by heptanal, propyl acetate, and butyl acetates were inhibitory (blue). Mitral/tufted cells recorded from distinct areas have different RCMs (Figures 4A–4E). These maps, by necessity, were only partial as limited recording time and long interstimulus intervals restricted the number of odorants that could be tested. However, they indicated that distance between the activated domains and the apical dendrites of the mitral/tufted cells critically determined the amplitude and sign of physiological responses of the underlying mitral/tufted cells. Strong depolarization and vigorous spiking were invariably correlated with activation of the region occupied by the tufts of apical dendrites (tilted rostrally and laterally away from somata), while odorants activating surrounding areas inhibited the cells or had no effect (Figures 4A–4E). Quantification of the effect of activated glomeruli at different distances from the glomeruli containing the tufts of the apical dendrites ($n = 8$; Figure 4F) strongly suggested that the RCMs of mitral/tufted cells generally have excitatory centers and inhibitory surrounds.

We further analyzed the correlation between cellular responses and the level of intrinsic signals at the location occupied by apical dendrites. For mitral/tufted cells with identified apical dendrites ($n = 8$), the location of their apical dendrite tufts within the maps of intrinsic signals was determined by the distance between apical dendrites and somata in mediolateral and anterioposterior directions. The level of intrinsic signals in the area of apical dendrites was calculated by averaging the values within an area of 10×10 pixels ($\sim 50\ \mu m \times 50\ \mu m$). The level of intrinsic signals within the area of apical dendrites was highly correlated with both the membrane potential changes ($r = 0.52$, $p < 0.001$; Figure 4G) and firing frequency changes ($r = 0.45$, $p < 0.01$) of neurons extending the apical dendrites. We next aligned the maps of receptive fields by centering images on the recording sites and then averaging the maps for all mitral cells, including those of which the apical dendrite was not recovered (data not shown). The consensus region correlated with greatest effectiveness in eliciting excitatory responses was centered $\sim 300\ \mu m$ anterior and $\sim 200\ \mu m$ lateral to the electrode penetration site, which was approximately the average displacement between the apical tufts of mitral cells and their parent somata. For all cells, the level of intrinsic signals within this area was highly correlated with the cellular responses in terms of both membrane potential change ($r = 0.46$, $p < 0.001$) and firing frequency change ($r = 0.31$, $p < 0.001$; $n = 33$ for mitral cells and $n = 122$ for tested trials of odorants). In contrast, neuronal responses were only very weakly correlated with the intrinsic signals directly above the somata ($r = 0.10$, $p = 0.27$ for membrane potential changes and $r = 0.17$, $p = 0.05$ for firing rate changes).

The responses of mitral cells to odorants activating domains distant from the apical dendrite termination zone of apical dendrites were more heterogeneous. Odorants activating glomeruli close to the apical dendritic territories elicited responses that were either weakly excitatory or inhibitory. Inhibitory responses were primarily observed for odorants activating areas clearly outside of the apical dendritic territories. The effective inhibitory distance between the activation areas and the location of mitral cells recorded in the dorsal

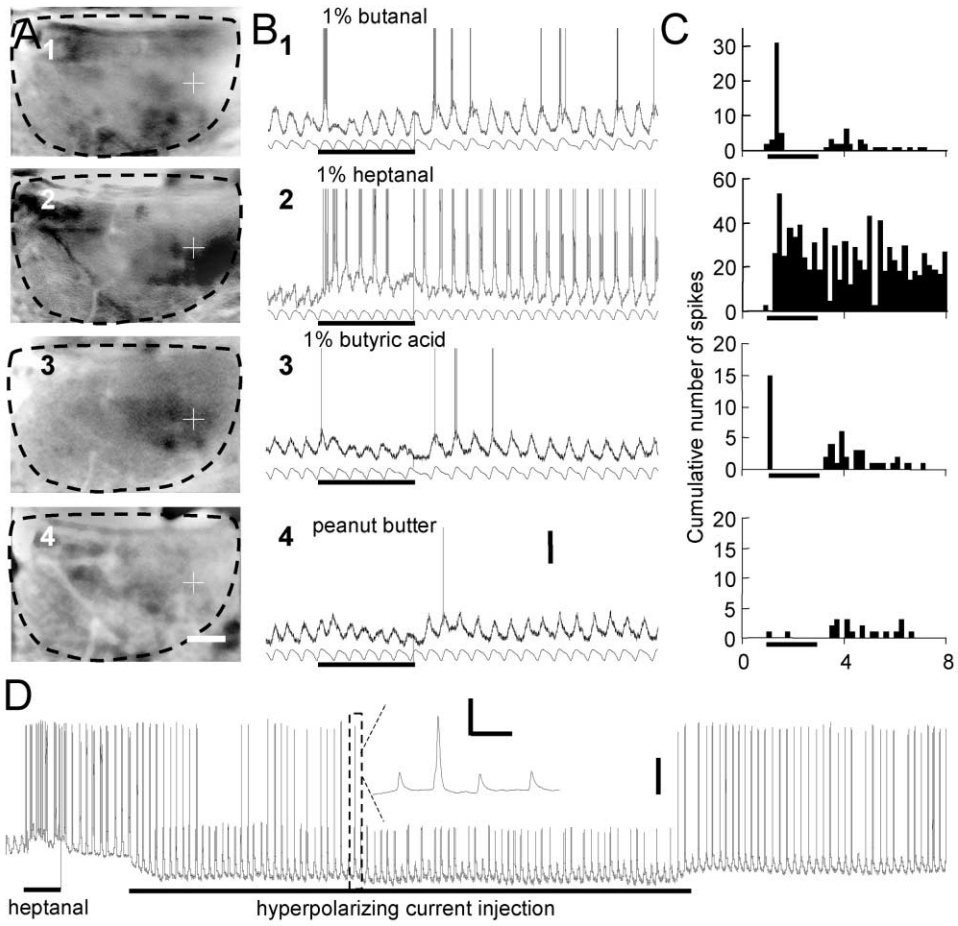

Figure 3. Glomerular Activation Patterns and the Response Profiles of Tufted Cells

(A) Maps of intrinsic signals from an olfactory bulb following presentation of different odorants. These odorants activated a significant portion of the anterior bulb. Conventions as in Figure 1. Bar = 500 μm. (B) Intracellularly recorded responses of a superficial tufted cell to odorant application. Unlike mitral cells, the inhibitory responses in tufted cells were less prominent and short odorant pulses (2 s) evoked prolonged responses, which were synchronized with the breathing rhythm (shown below the traces of membrane potentials). Vertical bar = 10 mV. (C) Peri-stimulus time histograms of neuronal spiking activity in response to 4–10 odorant presentations. (D) Prolonged activation of the cell following a 2 s heptanal pulse (indicated by the bar). Inset indicates an example of small action potentials, one of which preceded a large action potential. Unlike large action potentials, these small potentials persisted during hyperpolarizing current pulses as indicated. Vertical Bar = 20 mV. Bars in inset = 40 mV and 10 ms. Action potentials in (D) were not trimmed.

layer could be large (e.g., heptanal in Figure 2B). Even some mitral/tufted cells (n = 4/7) recorded from the ventral side of bulbs were reliably inhibited by aliphatic aldehydes (1%), some of which have been shown to activate discrete regions in the central and anterior areas of the dorsal bulb by both intrinsic signal imaging and 2-deoxyglucose labeling studies (Belluscio and Katz, 2001; Johnson and Leon, 2000b; Johnson et al., 1998). Butanal, heptanal, and amyl acetate clearly inhibited ventral cells and elicited a postinhibitory rebound following the end of odorant application, although the temporal patterns of the responses had some subtle differences (Figures 5A and 5B). Similar to mitral cells in the dorsal mitral cell layer, the apical dendrites of ventral mitral cells tilted rostrally and laterally (Figure 5C). These data suggest a center-surround organization within the RCMs of mitral/tufted cells, in which the excitatory center consists of a focal region surrounding the tufts of apical dendrites, and the inhibitory surrounds consists of a more extensive region of distant glomeruli.

Dynamics of Mitral/Tufted Cell Receptive Fields

We observed that mitral/tufted cells of mouse olfactory bulbs responded to odorant stimuli with complex response patterns including excitation (Figures 2C, $3B_2$, and $3B_4$), inhibition (Figures $1B_3$, 2B, $5A_3$, and $5A_4$), excitation followed by inhibition (Figures $5B_1$ and $5B_3$), and inhibition followed by excitation (Figures $1B_1$, $1B_2$, $5A_1$, and $5A_2$). Neurons also showed off-responses including either excitation or inhibition following excitation and postinhibitory rebound following inhibition. These temporal patterns are consistent with previous intra- and extracellular recording studies of olfactory response patterns in rodent mitral/tufted cells (Hamilton and Kauer, 1989; Meredith, 1986; Wellis et al., 1989). While static RCMs derived by averaging the overall response over the entire duration of odorant pulses had a center-surround structure, these complex temporal patterns of mitral/tufted cell responses suggested that the architecture of these maps could change during and after odorant presentation.

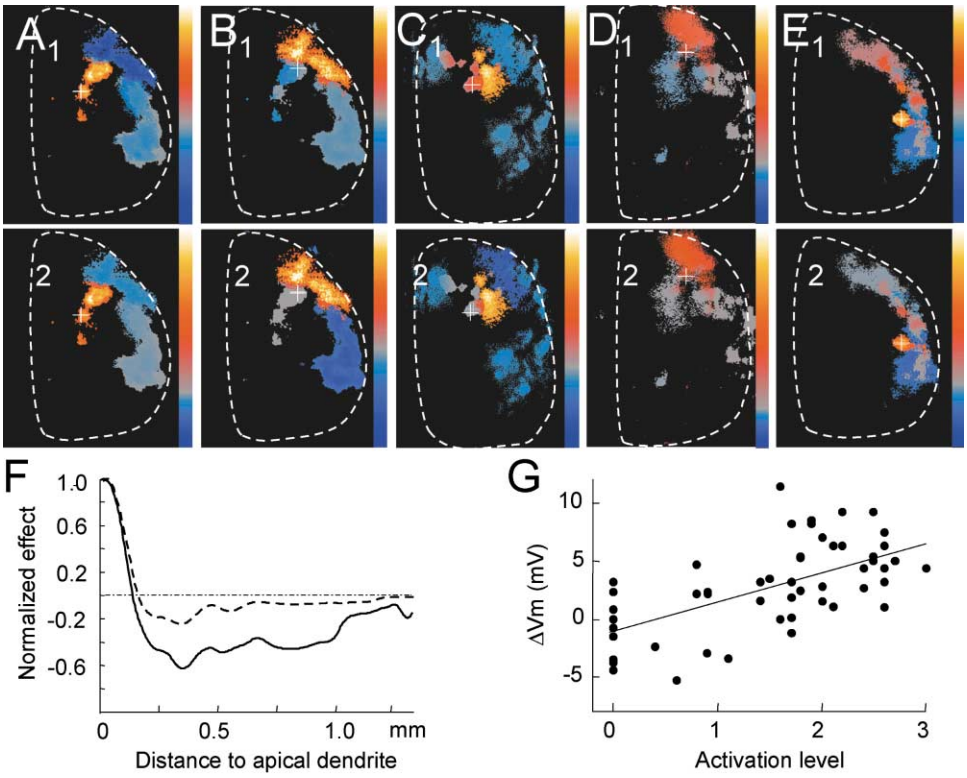

Figure 4. Center-Surround Structure within the Mitral/Tufted Cell Response Correlation Maps

(A) A response correlation map (RCM) for the cell shown in Figure 1 was constructed by correlating the intracellularly recorded responses to the activated domains of respective odorants. (A_1) RCM constructed by using the averaged membrane potential difference during and before odorant presentations. The color scale bar range for A_1 = (−7.6, 8.8), where −7.6 was the minimum (blue) and 8.8 was the maximum (white). For this and the following figures, zero value is represented by gray. Unit for this value is mV·STD, where STD is the standard deviation of intrinsic signals. (A_2) RCM constructed using changes in firing rate. These RCMs were characterized by a small central excitatory region and a much more extensive and weaker inhibitory surround. Conventions as in Figure 1. Range of color scale bar for (A_2) = (−12.5, 37.5) Hz·STD. (B) RCMs constructed for the cell shown in Figure 2C. Range of color bars in (B_1) = (−7.6, 7.6), (B_2) = (−17.5, 21.0). (C) RCMs for a mitral cell from a different animal illustrating center-surround organization. Color bar range in (C_1) = (−11.5 12.5), (C_2) = (−10.5, 18). (D) RCM for the tufted cell shown in Figure 3. Color bar range in (D_1) = (−7.6, 19.9), (D_2) = (−13.0, 58.0). (E) RCM for a second superficial tufted cell from a different animal, showing center-surround organization similar to that of mitral cells. For this cell, odorants tested include propanal, butanal, pentanal, heptanal, and butyl acetate (all 1%). Color bar range in (E_1) = (−7.6, 7.5), (E_2) = (−12.5, 31.5). (F) Plot of pixel values for maps of eight mitral/tufted cells based on the distance between pixels and the center of identified tufts of apical dendrite. The curves were smoothed by convolution with a Gaussian kernel (STD = 50 μm). Solid line represents the curve derived from the RCMs based on membrane potential and dashed line represents the curve derived from maps based on firing rate. These curves indicate a focal excitatory center from a region <200 μm from the tufts of apical dendrites and inhibitory surrounds extending over 1 mm. Curves were normalized to the center of apical dendrite tufts. Dashed horizontal line indicates zero. (G) Scatter plot of membrane potential change and the intrinsic signal levels within the estimated terminal zones of identified apical dendrites (n = 8), showing a significant correlation between neuronal responses and the levels of activation in their principal glomeruli. Line indicates linear fit.

To examine how the RCM structure of mitral/tufted cells evolved over time, we constructed maps using short time frames during and after odorant pulses. When the olfactory responses were parsed into 200 ms bins and correlated with intrinsic signal images, a very different picture of RCM organization emerged. At various time steps, these maps (dynamic maps) differed substantially from the map constructed from averaged responses during the entire period of odorant application (static maps). For some cells, the transitions during odorant application were smooth, and the basic patterns were similar to those of the static map (Figure 6A) (the static maps for this cell are shown in Figure 4A_1 and the physiological traces and maps of intrinsic signals are shown in Figure 1). For many other cells, however, maps during odorant application showed abrupt fluctuations (Figures 6B and 6C).

To quantify the overall change of dynamic maps compared to the static maps, we calculated the correlation coefficient between each map derived at 200 ms intervals and the maps constructed from the averaged physiological responses across the entire 2 s stimulus duration (e.g., each map within Figure 6A was correlated with the map in Figure 4A_1). For nearly half the cells examined (n = 5/12, Figure 7A_1), the initial maps were inversely correlated with the average static maps in terms of both membrane potential fluctuation and firing rate change. This most likely resulted from the brief inhibition preceding strong excitatory responses in many cells (Figures 1B_1 and 1B_2; Figures 6A–6C), similar to the response patterns commonly observed in some insect antennal lobe neurons (King et al., 2000). The maps for off-responses were also inversely correlated with the on-responses (Figure 7A), most likely because

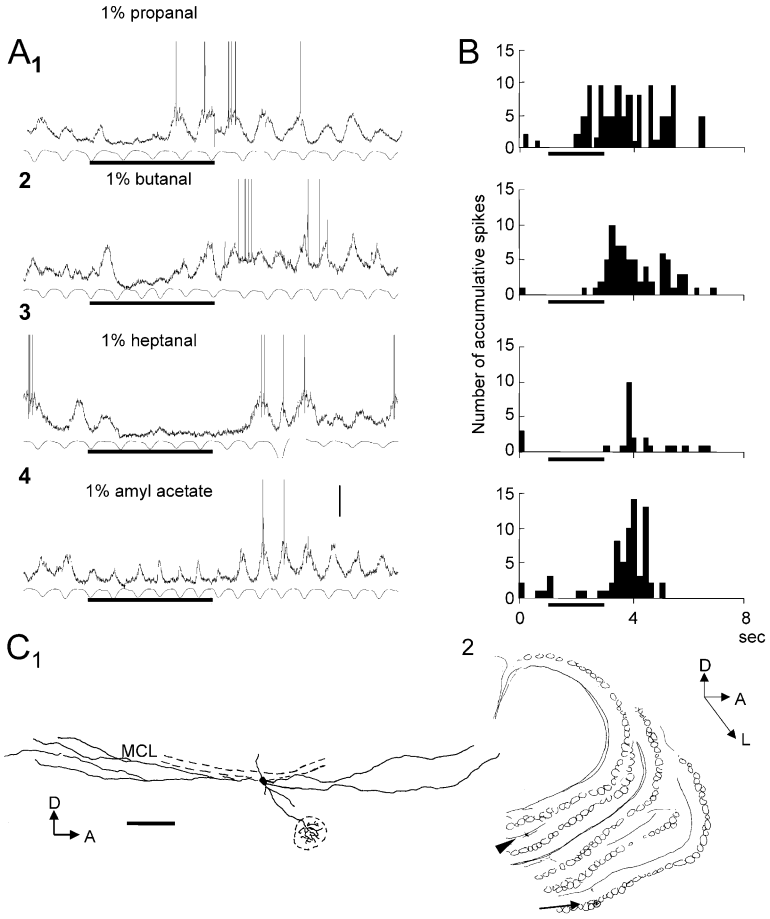

Figure 5. Long-Range Inhibition Suggested by the Response Profiles of Ventrally Located Mitral Cells

(A) Sample traces of membrane potential change of a ventrally located mitral cell to four odorants that activated glomeruli on the dorsal surface of the olfactory bulb. The responses were primarily inhibitory with conspicuous off-responses. Bars under the breathing rhythm indicate the timing of odorant pulses (2 s). Vertical bar = 10 mV. (B) Peristimulus time histograms of the cell's spiking activity in response to the odorants. Horizontal bar indicates 2 s odorant presentation. (C) Camera lucida reconstruction of the mitral cell, which was located within the ventral and lateral side of the bulb with its apical dendrite tilting toward a glomerulus anterior and lateral to the recording site. Adjacent parasagittal sections indicate the positions of the soma (arrowhead) and apical dendritic tuft (arrow) of the cell.

almost all of the inhibitory domains in the static maps became excitatory following the end of odorant pulses. This was probably due to release from inhibition (Figure 6). While many maps showed smooth transitions in the correlation coefficients (e.g., Figure $7A_1$), several showed rapid, abrupt change in the sign and degree of correlation (e.g., Figure $7A_2$), a consequence of dramatic changes in inhibitory domains in both sign and amplitude during odorant application (e.g., heptanal domains within the anterior bulbs for both cells in Figures 6B and 6C).

A key feature that emerged from averaging the group data (n = 12) was that RCMs became highly correlated to the static averaged map 400–600 ms (1–2 breathing cycles) after the initiation of odorant pulses; this high correlation ended ~600 ms after the end of odorant pulses (Figure $7B_1$). The variation in correlation among cells across time was initially high, reaching a minimum at about 2 s and quickly returning back to a high level of variation following the end of odorant pulses (Figure $7B_2$). For all cells examined (n = 12), RCMs at the initial phase of odorant application and those for off-responses differed substantially from the static maps (Figures 6A–6C).

Tuning of Granule Cells

The intracellularly recorded olfactory response patterns of granule cells (n = 10) were markedly different from those of mitral and tufted cells. While mitral/tufted cells typically responded strongly to some aldehydes or acetates (1%) with large membrane potential fluctuations and significant changes in firing frequency, granule cells responded only weakly. Membrane potential depolarizations were small (2–5 mV) as were increases in firing frequency (<5 Hz; Figures 8A, 8B, and 8D). Small spikes of short duration (half amplitude duration = ~2 ms) and variable amplitude (3–10 mV) were also frequently observed, occasionally preceding large action potentials (Figure $8B_4$ inset). These small spikes were not due to poor recording quality, as the size of action potentials was normal (Figure $8B_4$ inset) and odorants at high concentrations elicited strong responses (Figures $8B_2$ and $8B_3$); instead, they might reflect dendritic action potentials (Mori et al., 1982; Wellis and Scott, 1990). Similar to previous reports of granule cell response patterns in rat olfactory bulb (Wellis and Scott, 1990), we did not observe any convincing inhibitory effects on granule cells in response to odorants. Unlike mitral/tufted cells, granule cells had spiny dendrites projecting above the mitral cell layer and extending less than 150 μm horizontally (Figure 8C).

The olfactory response of granule cells was not strongly correlated to the activation of any single glomerular region, but rather appeared to be determined by the overall activation area (Figure 8D). In contrast to mitral/tufted cells, granule cells could be excited by odorants, which activated glomeruli 1 mm away from the electrode penetration site (Figure $8A_4$). Group data indicated no correlation between the intrinsic signals at

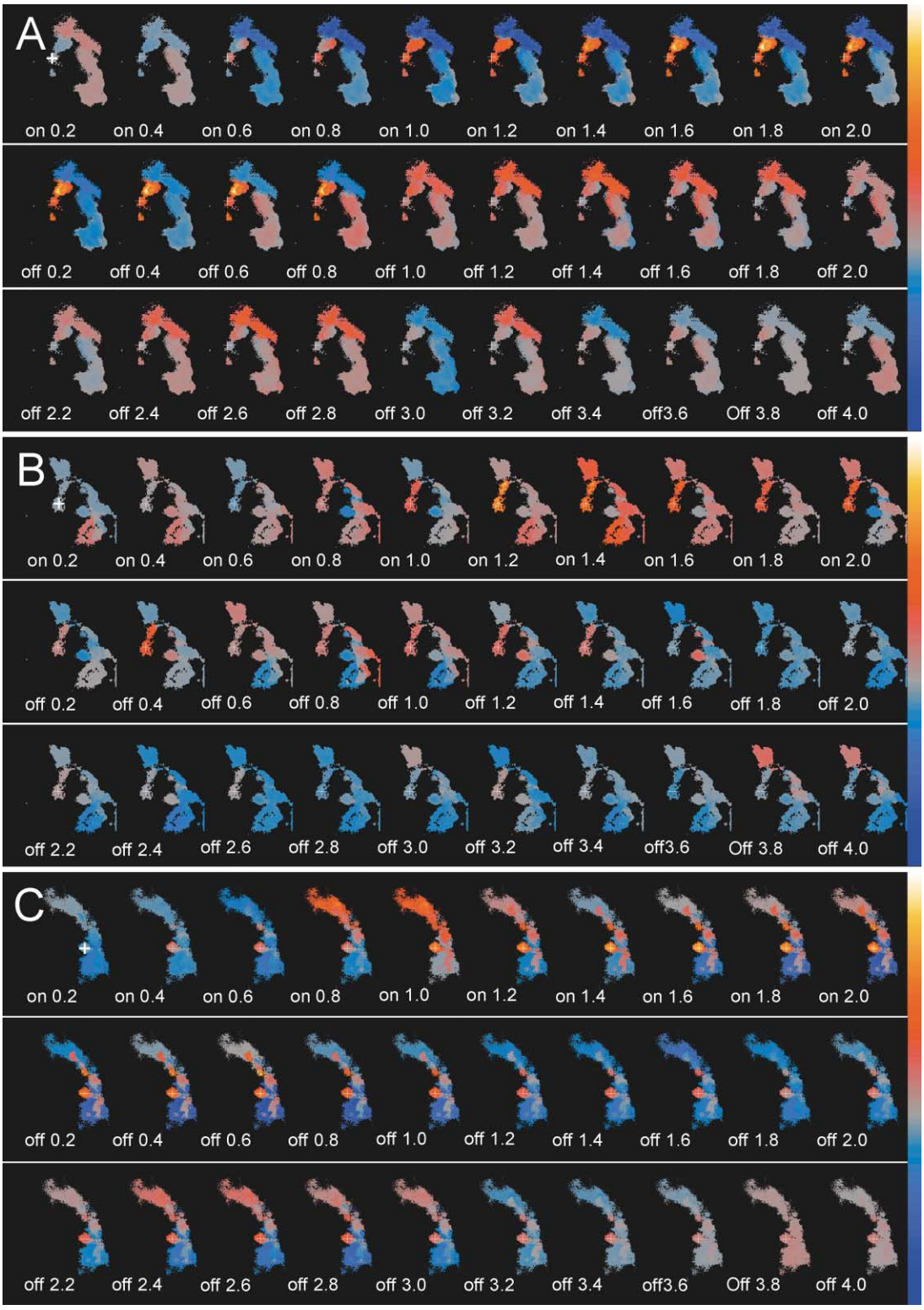

Figure 6. Time-Dependent Evolution of Response Correlation Maps

(A) Series of response correlation maps for the cell shown in Figures 1 and 4A including the times between the initiation of odorant pulses and 4 s after odorant pulses (total of 6 s, 30 frames). Maps were constructed by correlating the glomerular activation patterns as revealed by intrinsic signal imaging with the change in membrane potentials at different steps (each time frame = 200 ms) after the start of odorant pulses. The timing of each map is labeled within each map, where "on" indicates the time during odorant pulses and "off" indicates time after odorant pulses. The transitions between consecutive maps of this cell were smooth. Color scale bar range = (−18, 24). (B) Series of RCMs of a different mitral cell showing more abrupt transitions in map structure. Color bar range = (−7.6, 10). (C) Series of RCMs for a tufted cell shown in Figure 3E. Color bar range = (−7.9, 10).

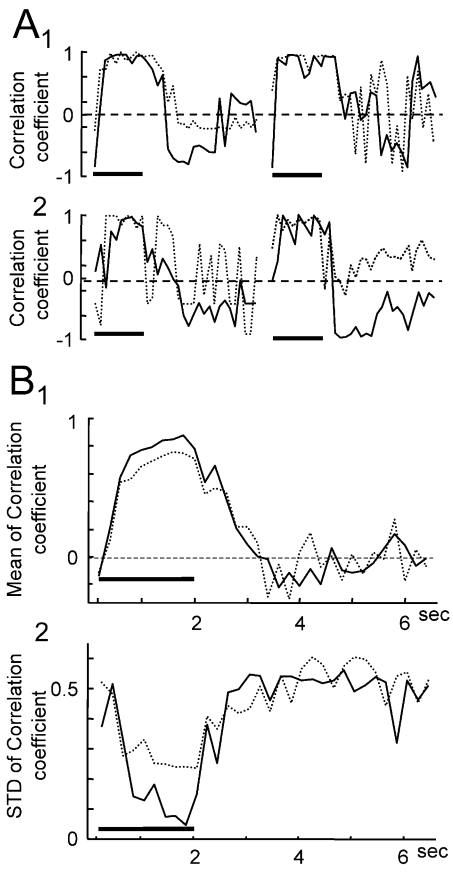

Figure 7. The Dynamics within the RCMs of Mitral/Tufted Cells

(A) The correlation coefficients between the maps at different time steps and the map constructed using the averaged physiological responses during the entire odorant pulses were calculated and plotted against time. (A_1) Two representative examples showing that correlation values initially were strongly negative but approached strong positive values (1.0) within a few hundred milliseconds. The left panel shows two curves that represent the change of correlation values between maps shown in Figure 6A and maps shown in Figure 4A. This high correlation continued for a few hundred milliseconds, became negative, and gradually returned to 0 following the end of odorant pulses. The right panel shows two curves that illustrate a similar inverse correlation at the onset and following the termination of odorant application. Solid curves indicate the correlation values for maps based on membrane potential change and dashed curves indicate those for maps based on firing rate change. Dashed horizontal lines indicate zero correlation. Horizontal bars below the curves indicate the timing of odorant pulses. (A_2) Two additional examples showing more dynamic evolution of correlation values both during and after odorant application. In these two examples, inverse correlations were not observed at the onset of odorant application for maps constructed with membrane potential change. (B_1) Averaged time-varying correlation values for 12 mitral/tufted cells. Overall, the maps constructed with 0.2 s time frame gradually evolved into a pattern highly similar to the maps constructed with physiological changes averaged across the entire 2 s duration. (B_2) Standard deviation of correlation values against time for the 12 mitral/tufted cells used to calculate the averaged correlation value.

the electrode penetration site and the membrane potentials changes to the odorants tested ($r = -0.02$, $p = 0.90$ for membrane potential change; $r = 0.22$, $p = 0.20$ for firing rate change; $n = 36$ for number of trials tested). Instead, the activity changes of granule cells were correlated with the extent of overall activated area ($r = 0.28$, $p = 0.10$ for membrane potential change; $r = 0.36$, $p < 0.05$ for firing rate change).

Discussion

In this study of the mouse olfactory bulb, we constructed response correlation maps by correlating the intracellularly recorded response patterns of mitral/tufted cells with spatial patterns of glomerular activation in response to different odorants. We found that mitral/tufted cells are strongly excited by odorants activating the glomerular areas innervated by their apical dendritic tufts, and are strongly inhibited by odorants activating nearby surrounding areas. This suggests that mitral/tufted cells have receptive fields consisting of an excitatory center and a largely inhibitory surround. Despite rich temporal patterns in the electrophysiological responses to odorants, the overall structure of response correlation maps of mitral/tufted cell evolves into a center-surround organization. Major changes occur both at the onset of and following the termination of odorant pulses.

Different Definitions of Olfactory Receptive Field

The receptive field is arguably one of the most fundamental concepts in studying sensory systems. In the visual system, for example, analysis of receptive field properties was essential for understanding the functional architecture of visual cortex (Hubel and Wiesel, 1968). Examining the receptive field structure is similarly important for understanding the function and organization of the olfactory system.

Defining olfactory receptive fields has proven difficult. The receptive field defined as effective epithelial areas (Jiang and Holley, 1992; Kauer and Moulton, 1974) is ultimately limited by the apparent random intermixing of receptor neurons within large epithelial zones (Ma and Shepherd, 2000; Malnic et al., 1999; Ressler et al., 1993). The receptive field defined as a set of responsive odorant molecules (Mori and Shepherd, 1994; Wilson, 2001) is conceptually straightforward and attractive. Studies based on this concept have provided important insights into the coding of molecular structures by bulbar and cortical neurons (Doving, 1966; Imamura et al., 1992; Katoh et al., 1993; Wilson, 2000). However, even studies using a large number of odorants, which inevitably affects the number of trials per odorant and limits the use of intracellular recording, can test only a small fraction of total possible odorant stimuli (Imamura et al., 1992; Katoh et al., 1993). Additionally, the dimensions and scales of the "odor space" are hardly quantifiable (Hopfield, 1999), resulting in great difficulty in mapping the organization of receptive fields.

Constructing the response correlation maps (RCMs) offers several advantages as a description of olfactory responses. Odorant identities are spatially mapped onto the glomerular layer (see Belluscio and Katz, 2001; Friedrich and Korsching, 1997; Johnson and Leon, 2000a; Meister and Bonhoeffer, 2001; Rubin and Katz, 1999; Yang et al., 1998; Uchida et al., 2000 for recent studies). RCMs of olfactory bulb neurons are therefore closely

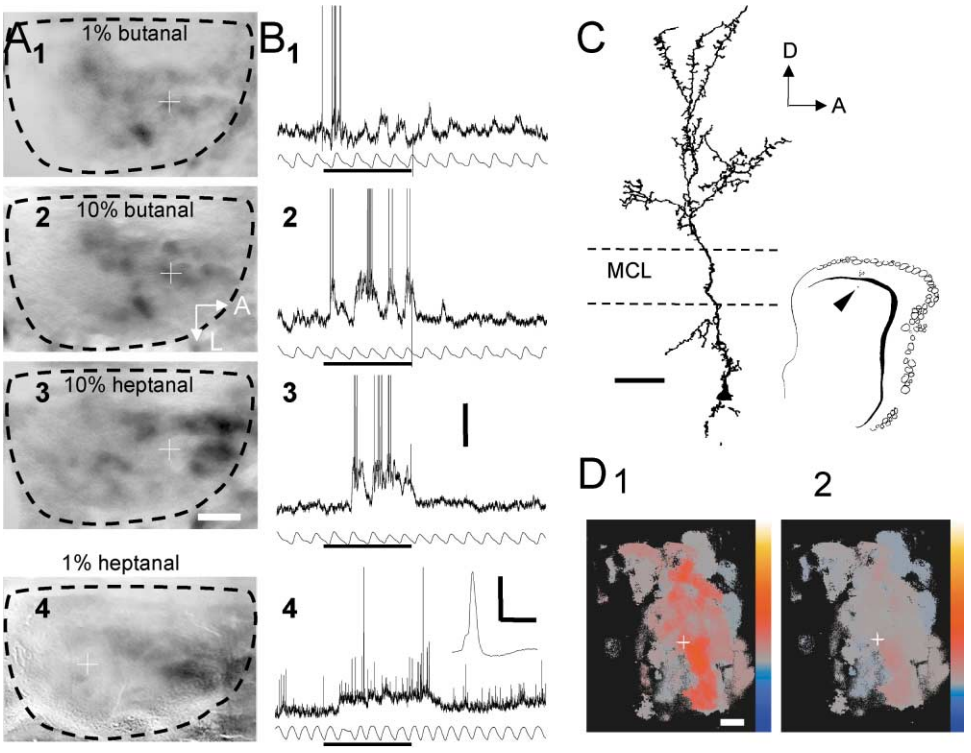

Figure 8. The Glomerular Activation Patterns and Olfactory Responses Profiles of Granule Cells

(A) Maps of intrinsic signals to 1% and 10% of butanal and heptanal. Crosshairs indicate electrode penetration sites. Maps 1–3 belong to same animal. Map 4 shows the map from a different animal for the purpose of comparison. Note odorants of higher concentrations recruited more glomeruli (Rubin and Katz, 1999). (B) Sample traces of granule cell responses recorded at the electrode penetration site shown in (A) in response to presentation of same odorants used for imaging. Granule cells exhibited weak responses to 1% odorant pulses but strong responses to 10% odorant pulses. Granule cells could be excited by odorants that activated regions distant from the recording sites. Inset shows a closer view of the trace within the dashed box where one large action potential was preceded by a small action potential. Unlike those observed in mitral/tufted cells, small action potentials of granule cells had variable and smaller amplitudes (3–10 mV). Horizontal bar in (B) = 2 s. Vertical bar in (B_3) = 10 mV and applies to all traces in (B) except the inset in (B_4), where bars = 40 mV and 10 ms. (C) Camera lucida drawing of the granule cell shown in (B_4). Granule cells typically had spiny dendrites extending to the outer plexiform layer. Inset is a camera lucida drawing showing the location of the granule cell soma (arrowhead). Bar = 40 μm. (D) Composite RCMs for all granule cells (n = 10) recorded in the dorsal part of olfactory bulbs, showing broad responsive glomerular areas, which contrast with the center-surround organization seen in mitral/tufted cells. (D_1) RCM based on the averaged membrane potential change evoked by odorant application. (D_2) RCM based on firing rate change. Crosshairs indicate the consensus location of electrode penetration sites. Maps for each granule cell were aligned by recording sites and averaged to produce a composite map for all granule cells. Bar = 500 μm. Color scale bar range for (D_1) = (−3, 6), for (D_2) = (−5, 15).

linked to the molecular receptive range of glomeruli. In addition, the glomerular layer contains the entire set of stimuli for bulbar and cortical neurons and is thus well defined. The spatial location of glomeruli is easily quantifiable. More importantly, advancement in imaging techniques allows in vivo visualization of glomerular activation patterns in a reasonably short time. Theoretically, by combining imaging, electrophysiological recordings, and reconstruction of cell morphology, it is possible to determine the response correlation map of any individual neuron.

Center-Surround Structure within Mitral/Tufted Cell RCMs

Our correlation study strongly suggests that RCMs and thus the receptive fields of mitral/tufted cells have a center-surround organization. The spatial patterns of glomerular activation clearly have a strong impact on the response patterns of underlying mitral/tufted cells (Figures 1–3). Moreover, the excitation of mitral cells is significantly correlated with the level of activation within a focal region surrounding their associated glomerulus (Figures 1 and 4; Buonviso et al., 1991), strongly suggesting an excitatory center within the mitral/tufted cell receptive field. Finally, we found that mitral/tufted cells are mainly inhibited by odorants activating glomerular domains not associated with the tufts of their apical dendrites (Figures 1–5), suggesting an inhibitory surround. Because of the difficulty of testing large numbers of odorants during intracellular recording, we only stimulated dorsoanterior and dorsolateral parts of the bulb and the maps were therefore only partial. Odorant application tended to activate multiple glomeruli, in some cases leading to the artifact of extended excitatory center that might in fact be inhibitory. The averaged on-center was smaller than those observed in the RCMs of

many individual cells (Figure 4F), suggesting that future studies may be able to reveal more complete RCMs of finer structures by using a larger set of odorants and lower odorant concentrations or by combining intracellular recording with in vivo application of photostimulation techniques (Katz and Dalva, 1994).

The center-surround structure of RCMs of mitral/tufted cells is shaped by the integration of input from receptor neurons and intrinsic processing within the olfactory bulb. Studies combining intrinsic signals and physiological recordings in cortex reveal close correlation between intrinsic signals and increases in neuronal activity (Grinvald et al., 1986; Maldonado et al., 1997). In the olfactory bulb, intrinsic signals are believed to represent neural activity of the glomerular layer that can be quantitatively accounted for by the affinity of receptor neurons (Meister and Bonhoeffer, 2001). Consistency between maps of intrinsic signals and maps based on other techniques further strengthens the validity of using intrinsic signals to represent glomerular activation (reviewed in Xu et al., 2000). The strong correlation between intrinsic signals and neuronal responses of mitral/tufted cells (Figure 4G) suggests that the excitatory on-center most likely reflects activation of receptor neurons projecting to the glomerulus containing the tufts of the mitral/tufted cell's apical dendrites.

The inhibitory surrounds of the RCMs of the mitral/tufted cell are consistent with the extensive lateral inhibition present within the olfactory bulb. Mitral/tufted cells form dendrodendritic synapses with GABAergic granule cells and receive reciprocal inhibitory feedback from the activation of more distant mitral/tufted cells (Jahr and Nicoll, 1980; Nowycky et al., 1981; Rall et al., 1966). Odorant presentation or electrical stimulation of the olfactory nerve layer evokes large inhibitory responses in mitral/tufted cells (Ezeh et al., 1993; Meredith, 1986; Wilson and Leon, 1987), supporting a role for lateral inhibition in patterning the olfactory responses of bulbar neurons. Mitral/tufted cells respond to specific features of odorant molecules (Imamura et al., 1992; Katoh et al., 1993), and blockade of GABAergic receptors unmasks excitatory responses to previously ineffective or even inhibitory odorants (Margrie et al., 2001; Yokoi et al., 1995), again implicating lateral inhibition in olfactory tuning. Lateral inhibition is thus probably a central mechanism underlying the center-surround organization of mitral/tufted cell receptive fields. The receptive fields of granule cells are much broader (Figure 8), probably because granule cells integrate excitation from large numbers of mitral cells through extensive dendrodendritic connections. Pharmacological manipulations of the circuitry can be used to examine the mechanisms underlying the extent and shape of the inhibitory surrounds.

The RCMs of mitral/tufted cells resemble the center-surround receptive fields of on-type retinal ganglion cells (Kuffler, 1953) and the relay neurons of the lateral geniculate nucleus (Wiesel and Hubel, 1966). The basic mechanisms of signal processing may be similar at an early stage of both the visual and olfactory systems (Mori and Shepherd, 1994). Nevertheless, mitral/tufted cells are different from retinal ganglia cells in that the long-range inhibition is recruited by odorants activating distant glomerular areas (Figures 1B_5, 2C, and 5). This suggests that lateral inhibition within the olfactory bulb may not be limited to increasing contrast of local features but can perform more global functions, such as synchronization of neuronal activity (Kashiwadani et al., 1999).

Intrinsic Dynamics within the Mitral/Tufted Cell RCMs

Neuronal receptive fields have dynamic spatiotemporal structures and the dynamics are exhibited at different levels. In the visual system, the receptive fields of cortical neurons can change over minutes to days in response to context and experience (Gilbert et al., 1996). In the olfactory cortex, repetitive odorant application results in habituation of cortical neurons, demonstrating the existence of similar dynamics in olfactory response properties at a slow time scale (Wilson, 2000).

In addition to slow changes, sophisticated mapping techniques have revealed rapid changes in receptive field structure at a subsecond time scale in other sensory systems (Dawis et al., 1984; Jenison et al., 2001; Jones and Palmer, 1987). Mouse mitral/tufted cells, like those of other vertebrates, respond to odorants with various temporal patterns (Hamilton and Kauer, 1989; Meredith, 1986; Wellis et al., 1989). Here, we triggered odorant pulses at the same phase of animal's respiratory cycle, allowing response patterns of different odorants to be directly compared within a cell (Buonviso et al., 1996). Assuming that the glomerular activation patterns remain largely constant during the entire period of odorant presentation (Friedrich and Korsching, 1998), we used a mapping technique conceptually similar to the reverse-correlation method to examine the fast spatiotemporal structures within the RCMs at subsecond scale (200 ms; Figure 6).

Compared to the static maps averaged across the entire duration of odorant pulses, maps of shorter time frames (200 ms) differed mainly during the onset and following the termination of odorant pulses. The olfactory responses of many mitral/tufted cells are modulated by respiratory rhythms (Buonviso et al., 1992; Wellis et al., 1989; Chalansonnet and Chaput, 1998), although this modulation is weaker in mouse mitral cells (Margrie et al., 2001; Figures 1, 2, and 4 of this study). The bin duration (200 ms) used to construct dynamic maps was shorter than the duration of the respiratory cycle ($\sim$250–400 ms), thus the contributions of activity during inhalation and exhalation varied across bins. Additionally, animals changed respiration frequency in response to the application of some odorants (Figure 1B_1). It is thus possible that some of the dynamic changes seen in our correlation analysis (Figures 6 and 7) were introduced by different respiratory phases and cycles. Application of continuous odorant streams through nasal cavity of tracheotomized animals may in fact reveal smoother transitions in the response correlation maps.

One of the key features revealed by this correlation analysis (Figure 7) is that the RCMs of mitral/tufted cells, despite their initial inverse patterns and their possible modulation by respiratory cycle, quickly (within 400–600 ms) evolved into a center-surround pattern. In most cases, this center-surround structure rapidly collapsed following the end of odorant pulses, generating an inverse pattern for a few seconds. The kinetics of the

response are similar to that of Ca^{2+} transients in the apical dendrites of frog mitral cells (Delaney et al., 2001). Neuronal responses of populations of mitral cells in zebrafish have been examined to characterize the evolution of response strength to different odorants (Friedrich and Laurent, 2001). These mitral cells, unlike their mammalian counterparts, receive input from multiple glomeruli and the temporal patterns of their responses are highly modulated so that the relative strength of a single cell's response to different odorants shifts within 1–2 s. The receptive fields of these zebrafish cells, defined as sets of responsive odorants, evolves to optimally reduce the overlap of mitral cell activation patterns to different odorants. The rodent olfactory bulb has a much larger number of glomeruli, each of which connects exclusively with a set of mitral/tufted cells (Baier and Korsching, 1994; Mori et al., 1999; Yoshihara et al., 2001). The center-surround structure of mitral/tufted cell RCMs leads to the activation of discrete populations of mitral/tufted cells in response to odorant application, which may serve to reduce overlap among the mitral/tufted cells in response to different odorants.

The intrinsic dynamics within the RCMs could have a computational role in olfactory coding. Dynamic receptive fields are believed to play an important role in signal processing of visual and auditory systems (DeAngelis et al., 1995; Jenison et al., 2001; McLean et al., 1994). Temporal response patterns of relay neurons in the honeybee antennal lobe are important for discriminating closely related odorants (Stopfer et al., 1997). Temporal patterns may also perform an important function for olfactory coding in other invertebrates (Christensen, et al., 2000) and vertebrates (Laurent, 1997; Mori et al., 1999). We find that the response patterns of mitral/tufted cells are closely correlated to spatial patterns of glomerular activation in mouse olfactory bulbs, suggesting that both spatial coding and temporal coding are employed in the initial stages of olfactory coding.

Experimental Procedures

Animals and Anesthesia

Adult (>7 weeks, 14–30 g) wild-type mice were used. All procedures used here were in accordance with a protocol approved by the Institutional Animal Care and Use Committee of Duke University. To reduce respiratory secretions, atropine (0.05 mg/kg, Ewlkins-Sinn, Cherry Hill, NJ) was used at the beginning of the experiment. Animals were anesthetized with 20% urethane solution (1.2 g/kg, Sigma-Aldrich, St. Louis, MO) and supplemented with a half-dosage as needed. Depth of anesthesia was monitored by heart rate change. Once anesthetized, animals were mounted in a custom-made stereotaxic apparatus and kept warm (39°C) with an electric heating pad. The breathing efforts of the animals were monitored by a strain gage (type KFG-3-120, Omega, Stamford, CT) affixed to chest skin with rubber cement. The strain gage was connected to a bridge module (BCM-1, Omega). Signals were amplified by a strain gage amplifier (DMD-465, Omega) and further filtered by a custom-made low pass filter (cutoff frequency = ~10 Hz).

Optical Imaging of Intrinsic Signals

Detailed procedures for optical imaging in the olfactory bulb have been described previously (Belluscio and Katz, 2001; Rubin and Katz, 1999). Briefly, the bone overlying the olfactory bulbs was thinned with a dental drill. Saline was perfused into a custom-made chamber to keep the thinned bone transparent. Images of the blood vessel patterns on the surface of the olfactory bulbs were acquired with green light (550 nm). For intrinsic signals imaging, the olfactory bulbs were illuminated with red light (630 nm) at near-saturation intensity. Following the start of odorant pulses, intrinsic signals were recorded and amplified using a commercial system (Imager2001, Optical Imaging Inc., NY). The maps of intrinsic signals were constructed by subtracting the averaged responses to mineral oil from the averaged responses to the odorant using the software provided by Optical Imaging Co. (Winmix 1.52). Signals were clipped at 3 standard deviations from mean and images were cropped; some images were further processed for presentation using a 3×3 median filter.

Odorants were diluted in mineral oil. Saturated vapors in charcoal filtered, desiccated room air were applied with pressure (2 l/min) using a TTL-triggered, 6-channel olfactometer. Using results from previous work as a guide, we chose odorants that activated different, in some cases overlapping, domains in substantial regions of the exposed bulb. The odorants included 1% or 10% saturated vapors of aliphatic aldehydes (3–8 hydrocarbon chains) and acetates (3–5 carbons; all from Sigma-Aldrich). Odorants were applied using Teflon tubing, the opening of which was placed ~2 cm from the nares. Odorant residues were quickly removed by a vacuum tube placed near animal's nose. The duration for each trial of odorant application was 10 s at 30–60 s interval. Each block contained 5–12 trials.

Electrophysiology

Optical maps were overlaid on the blood vessel images. A small hole was opened in the thinned skull on the dorsal bulb surface and the location was determined by the blood vessel pattern. Sharp intracellular recording electrodes (60–200 MΩ) filled with 2 M potassium acetate and 4% neurobiotin (Vector Laboratories, Burlingame, CA) were directed normal to the pial surface to search for cells. Signals from stable recordings were low pass filtered at 3 KHz, amplified (Axoclamp 2B, Axon Instruments, Union City, CA) and digitized at 6 KHz (National Instruments, Austin, TX). Traces of breathing rhythm and membrane potential change were simultaneously acquired for offline analysis. The input resistance of the cell was monitored with hyperpolarizing current pulses. Odorant pulses (2 s) were applied by opening the solenoid valves of the olfactometer, which was triggered by a specified point (usually the starting point of inhalation) within the monitored breathing rhythm. Because the shape of the breathing rhythm was nearly constant, triggering of odorant pulses allowed reliable timing of stimulus application relative to the breathing cycle throughout the recording session for each cell. Repetitive applications of the same odorants typically led to habituation and reduced the cell's responses, but crosshabituation by different odorants was infrequent (Wilson, 2000). To reduce habituation, the identities of the odorants were changed between trials and the inter-trial interval was at least 20 s. Data acquisition and experimental control were implemented by a customized Visual Basic program using driver programs provided by National Instruments.

Histology

Cells were filled with 4% neurobiotin by applying depolarizing currents. Within a large area (>1 mm^2), only a single cell recorded for at least 5 min was filled to facilitate later identification. Following the recording, the animal was sacrificed with Nembutal overdose, perfused with saline and 4% paraformaldehyde, and its brain was cryoprotected with 30% sucrose. Parasagittal sections (60 μm) were cut with a freezing microtome and reacted with 0.1% Alexa 488-streptavidin (Molecular Probes, Eugene, OR). Sections were mounted with mounting medium containing DAPI (H-1200, Vector Laboratories) to counterstain cell nuclei. Cell morphology was reconstructed by camera lucida drawing of several parasagittal sections. Glomeruli and layers within the olfactory bulbs were delineated by DAPI staining.

Data Analysis

Only cells recorded for over 10 min (mostly over 20 min, up to 2 hr) with stable membrane potential and input resistance, and at least some overshooting action potentials with spike amplitude >50 mV, were used for further analysis. Analysis was carried out using customized Matlab (Mathworks, Natick, MA) script programs.

To measure membrane potential fluctuation, digitalized physio-

logical traces were first filtered using a butterfly low pass filter (cutoff frequency = 60 Hz) to clip the action potentials and filter out other high-frequency components. This manipulation is similar to the operation of directly connecting the spike initiation point and after-hyperpolarization point (Carandini and Ferster, 2000) but is computationally faster. Although clipping action potentials can lead to underestimation of membrane potential fluctuations, it is nevertheless a good indicator of subthreshold activity, especially when the firing rate is low. Typically, 5–7 trials of membrane potential changes in response to the same odorant were averaged and the averaged trace was used to represent the patterns of membrane potential response of the cell to that odorant. Peri-stimulus time histograms of firing rates (200 ms per bin) were divided by the number of trials and were used to represent the firing rate change of the cell to the odorant.

Response Correlation Maps

To construct the RCMs, maps of intrinsic signals were cropped to exclude areas of intact bone and large blood vessels in the medial and posterior part of the bulbs. We then scaled the maps of intrinsic signals to ± 3 standard deviations (STD). The sign of the signals was reversed to ensure that activated areas had positive values, and the reversed maps were further clipped to the range of 0–3 STD by setting all negative pixel values to zero. Unlike the commonly presented maps of intrinsic signals, where activated areas have lower pixel values, these converted maps have higher values in the activated areas. The values of intrinsic signals at most pixels were not normally distributed because the frequency of activation was not even throughout the map and only limited number of odorants were tested. We therefore did not employ the standard definition of correlation coefficient between intrinsic signals and neuronal responses. Instead, the response correlation map *RCM* for each cell was defined as averaged correlation strength between neuronal responses and activated glomerular areas. RCM was constructed as following: $RCM = \Sigma_i(MI_i \times \Delta R_i)/\Sigma_i MT_i$, where i was the odorant index and MI_i was the map of intrinsic signals showing areas activated by odorant i. Activation was defined as glomerular areas which had levels of intrinsic signals greater than half of the peak values in activated oval areas for each individual map, or 1.0 STD if no activation were observed (overall threshold = 1.1 ± 0.2 STD). This threshold delineated activated regions of 50–200 μm diameter and was used in previous study to calculate the size of activated glomeruli (Rubin and Katz, 1999). The reduction of intrinsic signal strength was not reliable in our studies and its physiological implication, unlike that of activating intrinsic signals, is not clear (Grinvald et al., 1986; Meister and Bonhoeffer, 2001). We therefore excluded nonactivated areas by clipping the values of intrinsic signals lower than the thresholds to generate map MI_i. ΔR_i was the physiological response of the cell to the odorant pulse i. It was either the averaged values of membrane potential change or firing rate change within the 2 s of odorant pulse for static maps shown in Figure 4. The first step of RCM construction was to weight each map of activation MI_i with the physiological effect of odorant on the cell by multiplying the map by the values of either membrane potential change or firing frequency change. These newly weighted maps were then summed across different odorants as $\Sigma_i (MI_i \times \Delta R_i)$ to reveal the physiological responses to spatial patterns of glomerular activation. Because some areas within the maps were activated multiple times by different odorants, the pixel values within the map of accumulative weighted signals were divided by occurring frequency of activation $\Sigma_i MT_i$ to construct the final RCMs. Here *MTi* represented a binary map of activation, within which the pixel values were 1 if the value of the same pixel within the map MI_i is >0 following clipping.

Response correlation maps combined both values of neuronal responses and the levels of glomerular activation and essentially measured the correlation between these two values. Because the sign of the intrinsic signals was not negative and their amplitudes were limited to a small range (1–3 STD), the sign of the pixel values in the RCMs represented whether odorants activating the glomerular areas excited or inhibited cell and the amplitudes of the pixel values represent the scale of this effect. To accommodate the fact that only a limited set of odorants was applied and therefore some areas within the map were not tested, these areas were designated with special non-numerical values and are shown as black regions in the maps (for example, see Figure 4).

For dynamic maps, averaged values of membrane potential and firing rates within each 200 ms time frame were used. Each cell had a series of maps starting from the initiation of odorant pulses to a few seconds following the termination of the odorant pulses. Every map represented response correlation map between the glomerular activation patterns and neuronal responses within a 200 ms time frame at a certain time point. To examine the dynamics of RCM structures, we calculated the correlation coefficient between the RCMs for each time frame and the static map generated by using the physiological response across the whole duration of odorant pulses. The evolution of the RCM maps was plotted as the change of correlation coefficients over time.

Acknowledgments

We thank B. Rubin and L. Belluscio for their comments on the manuscript.

Received July 23, 2001; revised October 4, 2001.

References

Baier, H., and Korsching, S. (1994). Olfactory glomeruli in the zebrafish form an invariant pattern and are identifiable across animals. J. Neurosci. *14*, 219–230.

Belluscio, L., and Katz, L.C. (2001). Symmetry, stereotypy, and topography of odorant representations in mouse olfactory bulbs. J. Neurosci. *21*, 2113–2122.

Buonviso, N., Chaput, M.A., and Scott, J.W. (1991). Mitral cell-to-glomerulus connectivity: an HRP study of the orientation of mitral cell apical dendrites. J. Comp. Neurol. *307*, 57–64.

Buonviso, N., Chaput, M.A., and Berthommier, F. (1992). Temporal pattern analyses in pairs of neighboring mitral cells. J. Neurophysiol. *68*, 417–424.

Buonviso, N., Chaput, M.A., and Berthommier, F. (1996). Similarity of granular-induced inhibitory periods in pairs of neighboring mitral/tufted cells. J. Neurophysiol. *76*, 2393–2401.

Carandini, M., and Ferster, D. (2000). Membrane potential and firing rate in cat primary visual cortex. J. Neurosci. *20*, 470–484.

Chalansonnet, M., and Chaput, M.A. (1998). Olfactory bulb output cell temporal response patterns to increasing odor concentrations in freely breathing rats. Chem. Senses *23*, 1–9.

Christensen, T.A., Pawlowski, V.M., Lei, H., and Hildebrand, J.G. (2000). Multi-unit recordings reveal context-dependent modulation of synchrony in odor-specific neural ensembles. Nat. Neurosci. *3*, 927–931.

Cinelli, A.R., Hamilton, K.A., and Kauer, J.S. (1995). Salamander olfactory bulb neuronal activity observed by video rate, voltage-sensitive dye imaging. III. Spatial and temporal properties of responses evoked by odorant stimulation. J. Neurophysiol. *73*, 2053–2071.

Dawis, S., Shapley, R., Kaplan, E., and Tranchina, D. (1984). The receptive field organization of X-cells in the cat: spatiotemporal coupling and asymmetry. Vision Res. *24*, 549–564.

DeAngelis, G.C., Ohzawa, I., and Freeman, R.D. (1995). Receptive-field dynamics in the central visual pathways. Trends Neurosci. *18*, 451–458.

Delaney, K.R., Davison, I., and Denk, W. (2001). Odour-evoked [Ca2+] transients in mitral cell dendrites of frog olfactory glomeruli. Eur. J. Neurosci. *13*, 1658–1672.

DeMonasterio, F.M. (1979). Asymmetry of ON- and OFF-pathways of blue-sensitive cones of the retina of macaques. Brain Res. *166*, 39–48.

Doving, K.B. (1966). An electrophysiological study of odour similarities of homologous substances. J. Physiol. *186*, 97–109.

Ezeh, P.I., Wellis, D.P., and Scott, J.W. (1993). Organization of inhibition in the rat olfactory bulb external plexiform layer. J. Neurophysiol. *70*, 263–274.

Friedrich, R.W., and Korsching, S.I. (1997). Combinatorial and chemotopic odorant coding in the zebrafish olfactory bulb visualized by optical imaging. Neuron *18*, 737–752.

Friedrich, R.W., and Korsching, S.I. (1998). Chemotopic, combinatorial, and noncombinatorial odorant representations in the olfactory bulb revealed using a voltage-sensitive axon tracer. J. Neurosci. *18*, 9977–9988.

Friedrich, R.W., and Laurent, G. (2001). Dynamic optimization of odor representations by slow temporal patterning of mitral cell activity. Science *291*, 889–894.

Gilbert, C.D., Das, A., Ito, M., Kapadia, M., and Westheimer, G. (1996). Spatial integration and cortical dynamics. Proc. Natl. Acad. Sci. USA *93*, 615–622.

Grinvald, A., Lieke, E., Frostig, R.D., Gilbert, C.D., and Wiesel, T.N. (1986). Functional architecture of cortex revealed by optical imaging of intrinsic signals. Nature *324*, 361–364.

Hamilton, K.A., and Kauer, J.S. (1989). Patterns of intracellular potentials in salamander mitral/tufted cells in response to odor stimulation. J. Neurophysiol. *62*, 609–625.

Hopfield, J.J. (1999). Odor space and olfactory processing: collective algorithms and neural implementation. Proc. Natl. Acad. Sci. USA *96*, 12506–12511.

Hubel, D.H., and Wiesel, T.N. (1968). Receptive fields and functional architecture of monkey striate cortex. J. Physiol. *195*, 215–243.

Imamura, K., Mataga, N., and Mori, K. (1992). Coding of odor molecules by mitral/tufted cells in rabbit olfactory bulb. I. Aliphatic compounds. J. Neurophysiol. *68*, 1986–2002.

Jahr, C.E., and Nicoll, R.A. (1980). Dendrodendritic inhibition: demonstration with intracellular recording. Science *207*, 1473–1475.

Jenison, R.L., Schnupp, J.W., Reale, R.A., and Brugge, J.F. (2001). Auditory space-time receptive field dynamics revealed by spherical white-noise analysis. J. Neurosci. *21*, 4408–4415.

Jiang, T., and Holley, A. (1992). Some properties of receptive fields of olfactory mitral/tufted cells in the frog. J. Neurophysiol. *68*, 726–733.

Johnson, B.A., and Leon, M. (2000a). Modular representations of odorants in the glomerular layer of the rat olfactory bulb and the effects of stimulus concentration. J. Comp. Neurol. *422*, 496–509.

Johnson, B.A., and Leon, M. (2000b). Odorant molecular length: One aspect of the olfactory code. J. Comp. Neurol. *426*, 330–338.

Johnson, B.A., Woo, C.C., and Leon, M. (1998). Spatial coding of odorant features in the glomerular layer of the rat olfactory bulb. J. Comp. Neurol. *393*, 457–471.

Jones, J.P., and Palmer, L.A. (1987). The two-dimensional spatial structure of simple receptive fields in cat striate cortex. J. Neurophysiol. *58*, 1187–1211.

Kashiwadani, H., Sasaki, Y.F., Uchida, N., and Mori, K. (1999). Synchronized oscillatory discharges of mitral/tufted cells with different molecular receptive ranges in the rabbit olfactory bulb. J. Neurophysiol. *82*, 1786–1792.

Katoh, K., Koshimoto, H., Tani, A., and Mori, K. (1993). Coding of odor molecules by mitral/tufted cells in rabbit olfactory bulb. II. Aromatic compounds. J. Neurophysiol. *70*, 2161–2175.

Katz, L.C., and Dalva, M.B. (1994). Scanning laser photostimulation: a new approach for analyzing brain circuits. J. Neurosci. Methods *54*, 205–218.

Kauer, J.S. (1988). Real-time imaging of evoked activity in local circuits of the salamander olfactory bulb. Nature *331*, 166–168.

Kauer, J.S., and Moulton, D.G. (1974). Responses of olfactory bulb neurones to odour stimulation of small nasal areas in the salamander. J. Physiol. *243*, 717–737.

King, J.R., Christensen, T.A., and Hildebrand, J.G. (2000). Response characteristics of an identified, sexually dimorphic olfactory glomerulus. J. Neurosci. *20*, 2391–2399.

Kuffler, S.W. (1953). Discharge patterns and functional organization of mammalian retina. J. Neurophysiol. *16*, 37–68.

Laurent, G. (1997). Olfactory processing: maps, time and codes. Curr. Opin. Neurobiol. *7*, 547–553.

Ma, M., and Shepherd, G.M. (2000). Functional mosaic organization of mouse olfactory receptor neurons. Proc. Natl. Acad. Sci. USA *97*, 12869–12874.

Maldonado, P.E., Godecke, I., Gray, C.M., and Bonhoeffer, T. (1997). Orientation selectivity in pinwheel centers in cat striate cortex. Science *276*, 1551–1555.

Malnic, B., Hirono, J., Sato, T., and Buck, L.B. (1999). Combinatorial receptor codes for odors. Cell *96*, 713–723.

Margrie, T.W., Sakmann, B., and Urban, N.N. (2001). Action potential propagation in mitral cell lateral dendrites is decremental and controls recurrent and lateral inhibition in the mammalian olfactory bulb. Proc. Natl. Acad. Sci. USA *98*, 319–324.

McLean, J., Raab, S., and Palmer, L.A. (1994). Contribution of linear mechanisms to the specification of local motion by simple cells in areas 17 and 18 of the cat. Vis. Neurosci. *11*, 271–294.

Meister, M., and Bonhoeffer, T. (2001). Tuning and topography in an odor map on the rat olfactory bulb. J. Neurosci. *21*, 1351–1360.

Meredith, M. (1986). Patterned response to odor in mammalian olfactory bulb: the influence of intensity. J. Neurophysiol. *56*, 572–597.

Mombaerts, P., Wang, F., Dulac, C., Chao, S.K., Nemes, A., Mendelsohn, M., Edmondson, J., and Axel, R. (1996). Visualizing an olfactory sensory map. Cell *87*, 675–686.

Mori, K., Nagao, H., and Yoshihara, Y. (1999). The olfactory bulb: coding and processing of odor molecule information. Science *286*, 711–715.

Mori, K., and Shepherd, G.M. (1994). Emerging principles of molecular signal processing by mitral/tufted cells in the olfactory bulb. Semin. Cell Biol. *5*, 65–74.

Mori, K., Nowycky, M.C., and Shepherd, G.M. (1982). Impulse activity in presynaptic dendrites: analysis of mitral cells in the isolated turtle olfactory bulb. J. Neurosci. *2*, 497–502.

Mountcastle, V.B. (1957). Modality and topographic properties of single neurons of the cat's somatic sensory cortex. J. Neurophysiol. *20*, 408–434.

Nowycky, M.C., Mori, K., and Shepherd, G.M. (1981). GABAergic mechanisms of dendrodendritic synapses in isolated turtle olfactory bulb. J. Neurophysiol. *46*, 639–648.

Rall, W., Shepherd, G.M., Reese, T.S., and Brightman, M.W. (1966). Dendrodendritic synaptic pathway for inhibition in the olfactory bulb. Exp. Neurol. *14*, 44–56.

Ressler, K.J., Sullivan, S.L., and Buck, L.B. (1993). A zonal organization of odorant receptor gene expression in the olfactory epithelium. Cell *73*, 597–609.

Rubin, B.D., and Katz, L.C. (1999). Optical imaging of odorant representations in the mammalian olfactory bulb. Neuron *23*, 499–511.

Stopfer, M., Bhagavan, S., Smith, B.H., and Laurent, G. (1997). Impaired odour discrimination on desynchronization of odour-encoding neural assemblies. Nature *390*, 70–74.

Uchida, N., Takahashi, Y.K., Tanifuji, M., and Mori, K. (2000). Odor maps in the mammalian olfactory bulb: domain organization and odorant structural features. Nat. Neurosci. *3*, 1035–1043.

Vassar, R., Chao, S.K., Sitcheran, R., Nunez, J.M., Vosshall, L.B., and Axel, R. (1994). Topographic organization of sensory projections to the olfactory bulb. Cell *79*, 981–991.

Wellis, D.P., and Scott, J.W. (1990). Intracellular responses of identified rat olfactory bulb interneurons to electrical and odor stimulation. J. Neurophysiol. *64*, 932–947.

Wellis, D.P., Scott, J.W., and Harrison, T.A. (1989). Discrimination among odorants by single neurons of the rat olfactory bulb. J. Neurophysiol. *61*, 1161–1177.

Wiesel, T.N., and Hubel, D.H. (1966). Spatial and chromatic interactions in the lateral geniculate body of the rhesus monkey. J. Neurophysiol. *29*, 1115–1156.

Wilson, D.A. (2000). Comparison of odor receptive field plasticity in the rat olfactory bulb and anterior piriform cortex. J. Neurophysiol. *84*, 3036–3042.

Wilson, D.A. (2001). Receptive fields in rat primary olfactory cortex. Chem. Senses *26*, 577–584.

Wilson, D.A., and Leon, M. (1987). Evidence of lateral synaptic inter-

actions in olfactory bulb output cell responses to odors. Brain Res. *417*, 175–180.

Xu, F., Greer, C.A., and Shepherd, G.M. (2000). Odor maps in the olfactory bulb. J. Comp. Neurol. *422*, 489–495.

Yang, X., Renken, R., Hyder, F., Siddeek, M., Greer, C.A., Shepherd, G.M., and Shulman, R.G. (1998). Dynamic mapping at the laminar level of odor-elicited responses in rat olfactory bulb by functional MRI. Proc. Natl. Acad. Sci. USA *95*, 7715–7720.

Yokoi, M., Mori, K., and Nakanishi, S. (1995). Refinement of odor molecule tuning by dendrodendritic synaptic inhibition in the olfactory bulb. Proc. Natl. Acad. Sci. USA *92*, 3371–3375.

Yoshihara, Y., Nagao, H., and Mori, K. (2001). Neurobiology. Sniffing out odors with multiple dendrites. Science *291*, 835–837.